Published in final edited form as:

Clin Cancer Res. 2020 September 15; 26(18): 5007–5018. doi:10.1158/1078-0432.CCR-18-1359.

Fibrotic Response to Neoadjuvant Therapy Predicts Survival in Pancreatic Cancer and is Measurable with Collagen-Targeted Molecular MRI

Derek J. Erstad[1,*], **Mozhdeh Sojoodi**[1,*], **Martin S. Taylor**[2,*], **Veronica Clavijo Jordan**[3,*], **Christian T. Farrar**[3], **Andrea L. Axtell**[1], **Nicholas J. Rotile**[3], **Chloe Jones**[3], **Katherine A. Graham-O'Regan**[3], **Diego S. Ferreira**[3], **Theodoros Michelakos**[1], **Filippos Kontos**[1], **Akhil Chawla**[1], **Shen Li**[1], **Sarani Ghoshal**[1], **Yin-Ching Iris Chen**[3], **Gunisha Arora**[1], **Valerie Humblet**[5], **Vikram Deshpande**[2], **Motaz Qadan**[1], **Nabeel Bardeesy**[1], **Cristina R. Ferrone**[1], **Michael Lanuti**[1], **Kenneth K. Tanabe**[1,**], **Peter Caravan**[3,4,**], **Bryan C. Fuchs**[1,**]

[1]Department of Surgery, Massachusetts General Hospital, Harvard Medical School, Boston, MA, United States

[2]Department of Pathology, Massachusetts General Hospital, Harvard Medical School, Boston, MA, United States

[3]Martinos Center for Biomedical Imaging, Massachusetts General Hospital, Harvard Medical School, Charlestown, MA, United States

[4]Institute for Innovation in Imaging, Massachusetts General Hospital, Boston, MA, United States

[5]Collagen Medical LLC, Belmont, MA

Abstract

Purpose: To evaluate the prognostic value of post-treatment fibrosis in human PDAC patients, and to compare a type I collagen targeted MRI probe, CM-101, to the standard contrast agent, Gd-DOTA, for their abilities to identify FOLFIRINOX-induced fibrosis in a murine model of PDAC.

Experimental Design: Ninety-three chemoradiation-treated human PDAC samples were stained for fibrosis and outcomes evaluated. For imaging, C57BL/6 mice were orthotopically implanted with PDAC cells and FOLFIRINOX was administered. Mice were imaged with Gd-DOTA and CM-101.

Correspondence: Derek J. Erstad, MD. 55 Fruit St., Boston, MA 02114, derstad@partners.org; Bryan C. Fuchs, PhD, 4245 Sorrento Valley Blvd., San Diego, CA 92121, Bryan.Fuchs@ferring.com; Kenneth Tanabe, MD. 55 Fruit St., Boston MA 02114, ktanabe@partners.org.

*Co-first authors

**Co-senior authors

Author Contributions:

DJE and MS performed animal imaging experiments, imaging analysis, tissue processing, and protein expression analyses, statistical analyses, figure and manuscript creation. DJE, MS, SL, SG, GA, LW, and BCF performed tumor injections, animal dosing, and histologic staining and analyses. CJ, DSF, and KAG helped with hydroxyproline analysis and probe biodistribution studies. CTF, BCF, YIC, and PC contributed to animal imaging and imaging analysis. TM, FK, AC, CRF, MST, and VD contributed to histologic analysis of murine and human tumor samples. VD, MQ, NB, CF, ML, VH, KKT provided expert clinical opinion and helped with manuscript creation. PC, BCF, KKT contributed to experimental design and manuscript creation.

Conflicts of Interest:

VH is an employee of Collagen Medical, LLC. PC has >5% equity in Collagen Medical, LLC, a company working to commercialize the CM-101 probe. BCF received a research grant through Collagen Medical, LLC.

Results: In humans, post-chemoradiation PDAC tumor fibrosis was associated with longer overall survival (OS) and disease-free survival (DFS) on multivariable analysis (OS p = 0.028, DFS p = 0.047). CPA increased the prognostic accuracy of a multivariable logistic regression model comprised of previously established PDAC risk factors (AUC CPA (−) = 0.76, AUC CPA (+) = 0.82). In multiple murine orthotopic PDAC models, FOLFIRINOX therapy reduced tumor weight ($p < 0.05$) and increased tumor fibrosis by collagen staining ($p < 0.05$). CM-101 MR signal was significantly increased in fibrotic tumor regions. CM-101 signal retention was also increased in the more fibrotic FOLFIRINOX-treated tumors compared to untreated controls (p=0.027), consistent with selective probe binding to collagen. No treatment-related differences were observed with Gd-DOTA imaging.

Conclusions: In humans, post-chemoradiation tumor fibrosis is associated with OS and DFS. In mice, our MR findings indicate that translation of collagen molecular MRI with CM-101 to humans might provide a novel imaging technique to monitor fibrotic response to therapy in order to assist with prognostication and disease management.

Keywords

pancreatic cancer; neoadjuvant; chemoradiation; fibrosis; FOLFIRINOX; collagen; MRI; CM-101

Introduction

Pancreatic ductal adenocarcinoma (PDAC) is a highly morbid cancer with a five-year survival less than 5%.[1] Surgical resection remains the only curative therapy with long-term survival after R0 resection approaching 25%.[2] Unfortunately, the majority of patients are diagnosed at an advanced stage, and only 10–15% of cases present with resectable disease.[3] Neoadjuvant chemoradiotherapy (CRT) has become a common treatment option for patients with borderline resectable or locally advanced disease as it can potentially downstage the tumor, expanding surgical indications, and has been associated with reduced node positivity.[4–11] Though the impact of this approach on overall survival (OS) is still being evaluated in prospective, randomized clinical trials, these promising results on surrogate endpoints have led to the increasing use of neoadjuvant CRT.[9,12]

Prognostication after neoadjuvant CRT remains a challenge, however, as current pathologic scoring systems for treatment response have limited correlation with survival.[13] CRT induces a dense fibrotic reaction in PDAC, replacing tumor mass with extracellular matrix, of which type I collagen is a major component. Regression grading systems are primarily based on assessment of residual adenocarcinoma in the fibrotic field but are limited by high inter-observer variability.[14,15] It may be that objective quantification of treatment-related fibrosis better predicts survival. In this study we test this hypothesis by evaluating the association between the fibrotic response to CRT and prognosis among a cohort of human PDAC patients.

A second issue arising from the use of neoadjuvant CRT is that contrast-enhanced computed tomography (CT) and magnetic resonance imaging (MRI) cannot distinguish residual cancer from newly fibrotic tissue; therefore, radiographic downstaging after neoadjuvant therapy is rarely observed even when evidence of cytotoxic activity is found during subsequent

pancreatic resection.[8,16–19] This principle similarly applies for unresectable or advanced PDAC, which accounts for the majority of cases. For these patients, clinicians are reliant on radiographic assessment of progression to guide therapy; however, in the absence of change in tumor size or new foci of metastatic disease, little information about treatment response can be gained from CT or MRI. Therefore, there is a growing unmet need for the development of non-invasive markers to measure treatment response.

We hypothesize that type I collagen molecular MRI can address this need by providing superior visualization of the fibrotic response to therapy, which serves as a surrogate measure of treatment response, compared to standard contrast-enhanced MRI. Type I collagen levels correlate with the degree of fibrosis, and its extracellular nature makes it easily targetable with molecular probes. Our group previously showed that collagen molecular MRI can be used to measure baseline fibrosis in pancreatic tumors.[20] In this prior study, we used the type I collagen probe, EP-3533, which is a linear gadopentetate (Gd-DTPA) chelate that has retention in bone and other tissues, and therefore lacks capacity for clinical translation.[20] Here, we use a novel type I collagen molecular probe, CM-101, which employs a more stable macrocycle gadoterate (Gd-DOTA) chelate with potential for use in humans.[21] Using an orthotopic, syngeneic murine model of pancreatic cancer, we evaluate the ability of CM-101 to measure changes in fibrosis in response to FOLFIRINOX chemotherapy in comparison to the non-specific contrast agent, Gd-DOTA.

Methods

Patients

All human studies were performed in accordance with U.S. Common Rule and were approved by our Institutional Review Board with appropriate written patient consent where necessary. We retrospectively analyzed tumor specimens and medical records of 93 patients with borderline resectable or locally advanced PDAC treated with neoadjuvant FOLFIRINOX and radiation therapy with capecitabine followed by successful surgical resection at the Massachusetts General Hospital between 2012 and 2017. Per institutional protocol, each cycle of FOLFIRINOX was administered over a 14-day course. Fluorouracil was administered as a 400-mg/m^2 bolus on day 1, then as a 2400-mg/m^2 continuous infusion over 46 hours. Leucovorin calcium, 400 mg/m^2, oxaliplatin, 85 mg/m^2, and irinotecan hydrochloride, 180 mg/m^2, were administered on day 1. Pegfilgrastim, 6 mg, was administered on day 4. Patients also received either short course (25 GyE in 5 treatments with protons or 30 Gy in 10 fractions with photons) or long course (50.4 Gy in 28 fractions) radiotherapy. Capecitabine, 825 mg/m2 twice daily, or fluorouracil continuous infusion, 225 mg/m2/d, was given Monday through Friday during radiotherapy. Further details of this neoadjuvant protocol have been previously described.[22] All patients except one completed the prescribed 4 cycles of chemotherapy, and 82% of patients completed an additional 4 cycles for a total course of 8 preoperative cycles prior to undergoing pancreatic resection. Patients were followed until last clinic visit if still alive or until date of death. Clinicopathologic factors were evaluated for prognostic significance. The primary outcome measures were OS and DFS. A flow diagram summarizing the study design and patient selection is displayed in Supplementary Figure 1.

Pathologic and Histochemical Analysis

Formalin-fixed samples were embedded in paraffin, cut into 5-μm-thick slices and stained with hematoxylin and eosin (H&E), Sirius Red, and antibodies for CD31 (1:200 Cell Signaling Technology Inc., MA, USA), alpha smooth muscle actin (αSMA) (1:100, Sigma-Aldrich St. Louis, MO) and cleaved-caspase-3 (1:200, Cell Signaling Technology Inc., MA, USA) according to standard protocols. Images were captured with a Nikon Eclipse microscope equipped with an Insight CMOS 5.1 digital camera. Whole slides were scanned using a NanoZoomer-SQ Digital slide scanner (Hamamatsu Photonics K.K, Japan). Two board-certified pathologists evaluated all paraffin-embedded tissue sections for resected tumor specimens and scored pathologic regression per 2018 College of American Pathologists (CAP) criteria.[23] Regression grades included the following: complete response = no viable tumor cells present; moderate response = single cells or small groups of cancer cells; minimal response = residual cancer outgrown by fibrosis; poor response = minimal or no tumor kill with extensive residual cancer. Sections with the highest residual tumor content were subsequently used for Sirius Red collagen staining and fibrosis quantification as measured by collagen proportional area (CPA). All image analysis was performed using ImageJ (Version 1.0, National Institutes of Health). A detailed description of the Sirius Red staining technique and fibrosis quantification are provided in Supplementary Methods. Hydroxyproline was quantified by HPLC analysis and expressed as amount per wet weight of tissue.[24–27]

Cell Culture

A mouse pancreatic cancer cell line (Hy15549) from Ptf1-Cre; LSL-KRAS-G12D; p53 Lox/+ mice on an inbred C57B6/L background was used to generate tumors. For a second orthotopic PDAC model, a mouse pancreatic cancer cell line (Han4.13) from Ptf1a-Cre; LSL-Kras-G12D; p53 flox/+ mice on an inbred FVB/n background was used to generate tumors.[28,29] Both cell lines were seeded on uncoated plastic dishes and grown in Dulbecco's Modified Eagle Medium (DMEM) with 1% penicillin/streptomycin and 10% fetal bovine serum (FBS). All experiments were performed between passage 1 and 8.

Pancreatic Cancer Model

All experiments were performed in accordance with the National Institutes of Health's Guide for the Care of Use of Laboratory Animals and approved by the Institution's Animal Care and Use Committee. Prior to any operative procedures, mice were anesthetized with a mixture of ketamine 100mg/kg and xylazine 10mg/kg by intraperitoneal injection. Pancreatic tumors were established by orthotopic injection of pancreatic cancer cells via a left flank incision using a 28-gauge syringe as previously described.[30] We established two different orthotopic PDAC models: Hy15549 cells were used in C57BL/6 mice, and Han4.13 were used in FVB mice. Cell preparation involved 10,000 cells mixed 1:1 with Matrigel for an injection volume of 10 μL. Tumors were allowed to grow to 4–8 mm in diameter over a period of 10 days, at which time, mice were randomly assigned to receive FOLFIRINOX (67 mg/kg leucovorin, 33 mg/kg fluorouracil, 33 mg/kg irinotecan and 3 mg/kg oxaliplatin) 2X a week by intraperitoneal injection or saline control. Mice were imaged on days 17–18 and immediately sacrificed for tissue analysis.

CM-101

CM-101 comprises a 17-amino-acid peptide, with a 10-amino-acid disulfide bridged cyclic core, conjugated to three Gd-DOTA moieties through amide linkages.[21] CM-101 has a longitudinal relaxivity (per Gd) of 11.1 ± 0.3 $mM^{-1}s^{-1}$ and transverse relaxivity of 18.1 ± 0.7 $mM^{-1}s^{-1}$ at 1.5 T. CM-101 has a binding affinity for human type I collagen of K_d = 3.6 μM, and binds to approximately 8–10 sites per collagen monomer.

MRI Protocol

Animals were anesthetized with 1–2% isoflurane with body temperature maintained at 37 °C. The tail vein was cannulated for intravenous delivery of contrast agent while the animal was positioned in the scanner in a custom designed cradle. Imaging was performed at 4.7T using a small-bore animal scanner (Bruker, Billerica, MA). Baseline 2D and 3D Fast Low Angle Shot (FLASH) images were acquired before and continuously for 30 minutes after injection of 10 μmol/kg CM-101. 2D FLASH image acquisition parameters were TE/TR=2.93/125 ms, flip angle FA=60°, FOV=33x33 mm, matrix=140x140, slice thickness = 1.0 mm, and 9 image slices. 3D FLASH image acquisition parameters were TE/TR=2.46/15 ms, FA= 40°, FOV=48x28x20 mm, matrix=192x112x80.[24,31] MR signal to noise ratio (SNR) was measured at 5, 10, 15, 18, 20, and 25 minutes after CM-101 or Gd-DOTA injection and the increase in SNR relative to the image acquired before probe injection was computed (% ΔSNR).[32] The area under the %ΔSNR curve ($AUC_{5–25}$) was also calculated (5–25 min post-injection), and was used to compare signal enhancement over time between probes and treatment conditions. For all imaging experiments, a minimum of 5 mice were used for each treatment group.

Retention Map

CM-101 selectively binds fibrotic tissues that contain high levels of type I collagen, resulting in delayed probe clearance that corresponds to reduced MR signal loss over time.[21] Therefore, the rate of MR signal loss may be used as a surrogate marker of tissue fibrosis. Based on this principle, MR signal retention maps were generated by measuring MR signal loss over time in tumor tissue on a pixel-wise basis using OsiriX™ imaging software (Bernex, Switzerland).

A percent of peak value was calculated by subtracting the residual MR signal recorded at 25 minutes post injection from the peak signal recorded at 5 minutes post injection, shown by the following formula:

$$\text{Percent of peak } (\%) = [1 - (SI_{ROI\ 5min} - SI_{ROI\ 25min})/SI_{ROI\ 5min}] * 100$$

SI = MR signal intensity

ROI = region of interest outlining tumor tissue

$SI_{ROI\ 5min}$ = Peak MR intensity in tumor tissue at 5 minutes post injection

$SI_{ROI\ 25min}$ = MR intensity in tumor tissue at 25 minutes post injection

Percent of peak values were displayed using a color scale and were superimposed over standard axial MR images of tumor obtained 25 minutes after contrast injection.

Probe Biodistribution Analysis

For the evaluation of relative probe uptake in various tissues, mice were co-injected via tail vein with equimolar concentrations of Eu-DOTA (30 nmol/g) and CM-101 (10 nmol/g, 30 nmol/g with respect to Gd) followed by animal sacrifice 25 minutes post-injection using a cardiac terminal blood withdrawal. Eu-DOTA has the same biodistribution as Gd-DOTA but is MRI silent. Muscle, pancreas, and tumor were isolated, weighed, and acid-digested. Europium and gadolinium levels were measured by inductively coupled plasma mass spectrometry (ICP-MS), and expressed as amount per wet weight of tissue.[21]

Statistical Analysis

Results are expressed as the mean ± 1 SD unless otherwise noted. Student's *t* test compared data between control and one experimental group. One-way ANOVA followed by post-hoc Tukey tests with 2-tailed distribution were performed to analyze data among groups of 3 or more. For human data, survival curves were plotted using the Kaplan-Meier method, with 95% confidence intervals calculated using Greenwood's formula. Unadjusted and multivariable analyses to identify prognostic markers of overall survival were performed using the Cox proportional hazard models. Logistic model discrimination and calibration was assessed using the c-index, and internal validation was performed by calculating an optimism-corrected c-index generated from 500 bootstrapped samples generated from the original sample with replacement. All tests were performed 2-sided, and a significance level of $p < 0.05$ was considered to indicate statistical significance. All statistical analyses were performed using Intercooled Stata software, version 12.0 (StataCorp, College Station, TX). Data were plotted using Prism 6 (GraphPad Software, La Jolla, Calif).

Results

Fibrotic Response to Neoadjuvant Chemoradiation Predicts Survival in Human PDAC

It is suspected that the degree of fibrotic response after neoadjuvant CRT positively correlates with survival, however, this assertion has not been previously validated. We analyzed medical records and tumor specimens of 93 patients with borderline resectable or locally advanced PDAC treated with neoadjuvant FOLIFIRINOX and external beam radiation therapy followed by surgical resection and compared tumor fibrosis levels with survival. The median cohort age was 62 years and 49 (51%) patients were female. At the study endpoint, 51 (55%) patients had died of disease with a median OS of 41.3 months and 3-year OS of 58%. The median DFS was 12.4 months. Kaplan-Meier survival curves for OS

and DFS for the cohort are displayed in Supplementary Figure 2A. Additional demographic and clinicopathologic details for the cohort are displayed in Table 1.

Sirius Red staining of tumor specimens was performed, and the percent collagen proportional area (CPA) was digitally quantified. Post-neoadjuvant tumor fibrosis levels were normally distributed with a mean CPA of 69.4 ± 8.0% (Figure 1A). There was no significant difference in tumor CPA between patients who received external beam radiotherapy (EBRT) (n = 81) or proton therapy (n = 12) (EBRT 69.8 ± 7.7% vs. proton 66.7 ± 9.9%, p = 0.21). We also evaluated the time interval from the initiation of neoadjuvant therapy to the date of surgery. The average interval was 220 ± 75 days. There was a positive correlation between this time interval and tumor CPA (m = 0.033, p = 0.003), however, there was marked variance (R^2 = 0.09) (Supplementary Figure 2B). We also compared the number of administered FOLFIRINOX chemotherapy cycles and tumor CPA. The range included 3–24 cycles, however, the vast majority of patients received 8 cycles. Again, there was a positive correlation between the number of cycles and tumor CPA (m = 0.83, p = 0.013), however, there was also marked variance (R^2 = 0.07) (Supplementary Figure 2C).

Representative histologic images of tumor sections separated by low [CPA < 61.4% (< 1 SD of the mean)], moderate [(61.4 – 77.4% (± 1 SD of the mean)], and high [(> 77.4% (> 1 SD of the mean)] fibrosis are displayed in Figure 1B. Demographic variables, clinicopathologic traits, and CPA were evaluated for prognostic significance by univariate analysis in which the primary outcome measures were OS and DFS (Table 1). CPA was significantly associated with greater OS (HR 0.94, p = 0.001) and DFS (HR 0.95, p = 0.009), and for both outcome measures, a 10% increase in CPA was associated with an approximately 50% reduction in risk of death or recurrence. When separated by low (< 61.4%), moderate (61.4 – 77.4%), or high fibrosis (> 77.4%), the median OS was 24.7, 41.3, and 55.4 months, respectively (p = 0.0072). The median DFS for these same groups was 8.2, 13.5, and 37.7 months, respectively (p = 0.031) (Figure 1C).

In contrast, elevated serum CA-19–9 level, large tumor diameter, T stage 3–4, N stage 1–2, poor response by pathologic regression grading, and presence of perineural invasion were associated with reduced survival. Covariates that were significant on univariate analysis were included in a multivariable COX proportional hazards model for survival, and only CPA and radiographic tumor diameter at diagnosis remained significantly associated with OS and DFS (Table 2).

To further evaluate the prognostic value of CPA, a logistic regression model comprised of significant covariates on univariate analysis was constructed, and a receiver operator characteristic (ROC) analysis was performed with and without CPA included as variable in the model (Figure 1D). The area under the curve (AUC) of the logistic regression model for median OS with CPA excluded was 0.76 and increased to 0.82 with CPA included. Similarly, the AUC for median DFS without CPA was 0.77 and increased to 0.80 with CPA. In both cases, CPA still added predictive value after accounting for other significant covariates in the model. Additional end points for the logistic model, including one-year, two-year, three-year, and five-year OS and DFS are displayed in Supplementary Table 1.

Currently, the two standard clinical methods for evaluating PDAC neoadjuvant treatment response include pathologic response grading and radiographic response scoring using RECIST (Response Evaluation Criteria In Solid Tumors). In our analysis, RECIST was not associated with OS or DFS as an independent variable on univariate analysis, which was expected given the observed process by which tumor tissue is replaced with fibrosis in response to neoadjuvant therapy. Moreover, there was no correlation between RECIST and CPA. In contrast, pathologic regression grading was significantly associated with both OS and DFS on univariate but not multivariate analysis. For patients with complete or moderate pathologic response (n = 47) the median OS was 52.0 months, while those with minimal or poor response (n = 46) had a median OS of 29.6 months (p = 0.0068) (Supplementary Figure 2D). The median DFS for these groups was 27 months vs. 9 months (p = 0.088), respectively.

We observed a significant correlation between pathologic regression grade and CPA (Figure 1E). We next inquired whether combining pathologic regression scoring and CPA quantification provided additional prognostic value as both techniques can be readily performed by a pathologist. Therefore, we first sought to determine a CPA threshold with optimal prognostic accuracy using ROC analysis for median OS and DFS time points. Using our previously derived logistic regression model, we performed a bootstrapping method with 500 replications, and the optimism-corrected c-index of our logistic model for median OS was 0.78 with a mean maximal Youden's index of 0.67, corresponding to a CPA of 68.3%. Using the same methodology for median DFS, the optimism-corrected c-index was 0.76 with a mean maximal Youden's index of 0.59, corresponding to a CPA of 68.8%. Based on this analysis, we used a rounded cutoff of 70%, and the median OS and DFS for patients with CPA < 70% (n = 48) were 29.2 and 9.1 months, respectively, while the median OS and DFS for patients with CPA ≥ 70% (n = 45) were 52.0 (p = 0.0036) and 21.9 months (p = 0.029), respectively (Supplementary Figure 2E).

Using this CPA threshold, it was found that patients with evidence of both pathologic regression (complete or moderate grades) and increased post-neoadjuvant tumor fibrosis (CPA ≥ 70%) experienced significantly better survival outcomes than patients who lack one or both of these tumor features (median OS 55 vs. 33 months, p = 0.0008; median DFS 37 vs. 11 months, p = 0.018) (Figure 1F).

Taken together, CPA is an objectively quantified prognostic marker for PDAC that provides additional predictive value when taking into consideration other significant prognostic covariates. In our cohort, CPA was more sensitive than pathologic regression grading for prognosis, and therefore, this marker might have clinical value for determining prognosis.

An Orthotopic Syngeneic Murine Model Recapitulates the Desmoplastic Response Observed in Human PDAC

Hy15549 cells injected into the body of the mouse pancreas produce a locally contained tumor approximately 7–10 mm in diameter by day 14 (Figure 2A). The tumor histologic features recapitulate common findings of human PDAC, including: a hypovascular core, abnormal ductular architecture, a robust desmoplastic response, and local invasion into surrounding normal pancreatic tissue (Figure 2B&C). The desmoplastic reaction is

associated with infiltration and proliferation of fibroblastic cells characterized by alpha-smooth muscle actin (αSMA) expression (Figure 2D), and dense extracellular matrix deposition, notably collagen type I (Figure 2C). Accordingly, the collagen proportional area (CPA) is significantly greater in tumor tissue compared to surrounding pancreas (19.7 ± 6.5% vs. 13.2 ± 4.9%, p = 0.022) (Figure 2E), which was corroborated by analysis of hydroxyproline content (460 ± 108 μg/g vs. 639 ± 101 μg/g, p = 0.0012) (Supplementary Figure 3A). The desmoplastic response observed in this model provides ideal substrate for evaluation of CM-101 collagen binding and fibrosis imaging.

CM-101 Provides Superior Pancreatic Tumor Enhancement Compared to Gd-DOTA

Mice were imaged continuously for 25 minutes after contrast injection, and quantitation of MR signal intensity in tumor and surrounding pancreatic tissue was measured on a pixel-wise basis. Peak signal intensity for both contrast agents was observed within five minutes after injection, with rapid renal clearance observed by imaging (Figure 3A&B). With CM-101, enhancing tumor regions had significantly greater signal intensity than surrounding pancreas at all time points, as measured by the percent change in signal-to-noise ratio (%ΔSNR), which was not observed with Gd-DOTA (Figure 3C&D). The peak difference in %ΔSNR between pancreas and PDAC tissues occurred at 10 minutes post injection (21.2 ± 16.3% for CM-101 vs. 5.4 ± 2.9% for Gd-DOTA, p = 0.06). Taken together, these findings indicate that only CM-101 could accurately distinguish fibrotic tumor tissue from surrounding pancreas by MR signal intensity, which was associated with a more clearly defined tumor border in the MR images. Lastly, tumors in our model system display robust peripheral enhancement with both probes, with minimal signal intensity observed centrally. A similar radiographic enhancement pattern is frequently observed with gadolinium-based MRI in human PDAC. CD31 Immunohistochemistry in orthotopic tumors reveals spatial discrepancy in tumor vascularity, with peripheral regions having greater blood vessel density than the central region (Supplementary Figure 3B). This trait is consistent with a hypovascular core, resulting in decreased probe penetration and the observed imaging pattern.

CM-101 Selectively Enhances Fibrotic Tumor Tissue

We evaluated the kinetics of tumor enhancement for Gd-DOTA and CM-101 by measuring MR signal loss over time. Percent ΔSNR values were measured at 5, 10, 15, 18, 20, and 25 minutes post probe injection and were normalized to peak enhancement at 5 minutes. We showed previously that normalizing to peak enhancement at 5 minutes post injection accounts for differences in tumor permeability. The subsequent area under the curve for each probe ($AUC_{5–25}$) was expressed as a percentage of the total area (Figure 4A). At 25 minutes post-injection, Gd-DOTA is cleared from the tumor whereas CM-101 is largely retained ($AUC_{5–25}$ 66.3 ± 11.4% vs. 86.6 ± 8.1%, p = 0.002), indicating selective binding and retention of CM-101 in the fibrotic tumor tissue. We confirmed these findings by performing a biodistribution analysis of probe uptake 25 minutes after equimolar (metal ion) injection of both probes via tail vein. To allow for unique identification of each probe, DOTA was chelated to Europium (Eu) instead of Gd. Tumor metal concentration was measured by mass spectrometry. By this approach, CM-101 was found at significantly higher concentrations than Eu-DOTA (41.3 ± 16.3 nmol/g vs. 23.9 ± 8.6 nmol/g, p = 0.0078), consistent with the

imaging findings (Figure 4B). In the normal pancreas, there was no difference in MRI $AUC_{5–25}$ between CM-101 and Gd-DOTA (CM-101 78.1 ± 7.0% vs. Gd-DOTA 78.5 ± 4.3 %, p = 0.90), which was expected given the low baseline collagen expression in pancreatic tissue (Figure 4C). Representative axial T1-weighted 2D-RARE images of pancreatic tumors imaged at five (peak signal) and 25 minutes post-injection of Gd-DOTA (Figure 4D) and CM-101 (Figure 4E) are shown. The corresponding signal retention maps display the relative MR signal intensity at 25 minutes post injection (normalized to peak intensity at 5 minutes) on a color-transformed, pixel-wise basis. Consistent with measured changes in %ΔSNR over time, DOTA has uniformly cleared from the tumor bed, whereas considerable CM-101 signal intensity remains.

FOLFIRINOX Treatment in Mice Reduces Tumor Size and Increases Tumor Fibrosis

Tumors treated with FOLFIRINOX chemotherapy responded robustly with gross evidence of necrosis and hemorrhage (Figure 5A). These tumors were significantly smaller by weight (0.43 ± 0.03 g vs. 0.52 ± 0.02 g, p = 0.036) (Figure 5B). Similar to findings in human PDAC, FOLFIRINOX treatment in mice was also associated with a significant increase in tumor fibrosis compared to untreated lesions as measured by CPA (20.7 ± 3.5% vs. 33.9 ± 6.1%, p < 0.0001) (Figure 5A&C). Finally, cleaved-caspase-3 staining was increased within FOLFIRINOX-treated lesions (23.5 ± 2.9% vs. 1.8 ± 1.3%, p < 0.0001), demonstrating increased carcinoma-specific apoptosis (Supplementary Figure 3C).

CM-101 Accurately Measures Changes in Tumor Fibrosis in Response to FOLFIRINOX Chemotherapy

In FOLFIRINOX-treated mice, CM-101 was associated with increased MR $AUC_{5–25}$ in enhancing tumor regions compared to Gd-DOTA (94.4 ± 5.3% vs. 72.0 ± 4.1%, p < 0.0001) (Figure 6A). FOLFIRINOX treatment was also associated with increased CM-101 MR $AUC_{5–25}$ in surrounding pancreatic tissue compared to Gd-DOTA, which was observable by 18 minutes post-injection (79.8 ± 11.1% vs. 65.1 ± 6.9%, p = 0.0054) (Figure 6B). Biodistribution analysis 25 minutes after equimolar injection of CM-101 and Eu-DOTA was notable for increased CM-101 uptake in both tumor (45.1 ± 9.0 nmol/g vs. 14.8 ± 4.2 nmol/g, p < 0.0001) and pancreas (27.5 ± 4.6 nmol/g vs. 8.4 ± 3.4 nmol/g, p < 0.0001), consistent with imaging findings (Figure 6C).

Representative axial T1-weighted 2D-RARE images of pancreatic tumors imaged at 5 and 25 minutes post-injection of CM-101 are shown for untreated and FOLFIRINOX-treated mice (Figure 6D&E). FOLFIRINOX treatment was associated with increased CM-101 ΔSNR at all time points compared to untreated tumors (Figure 6F), and this difference was visible on the corresponding signal retention maps (Figure 6D&E). The CM-101 MR $AUC_{5–25}$ was significantly increased with FOLFIRINOX treatment compared to the untreated mice (94.4 ± 5.3% vs. 86.6 ± 8.1%, p = 0.027) (Figure 6F). Biodistribution analysis showed significantly elevated levels of CM-101 in FOLFIRINOX-treated tumors compared to untreated tumors (normalized to muscle) (7.2 ± 2.6 vs. 4.7 ± 1.8, p = 0.014) (Figure 6G). Conversely, there was no difference in signal enhancement of normal pancreatic tissue between treatment groups ($AUC_{5–25}$ FOLFIRINOX 79.8 ± 11.1% vs. untreated 78.1 ± 7.0%, p = 0.69) (Figure 6H). This was corroborated by biodistribution

analysis of CM-101 uptake in pancreatic tissue of untreated and FOLFIRINOX-treated mice (normalized to muscle) (untreated 3.6 ± 2.7 vs. FOLFIRINOX 4.4 ± 1.5, p = 0.37) (Figure 6I).

With Gd-DOTA, there was no difference in tumor MR $AUC_{5–25}$ between treatment groups (FOLFIRINOX 72.0 ± 4.1% vs. untreated 66.3 ± 11.8%, p = 0.21) (data not shown). Similarly, there was no difference between treatment groups regarding biodistribution of Gd-DOTA uptake in tumor tissue (normalized to muscle) (FOLFIRINOX 3.1 ± 0.3 vs. untreated 4.8 ± 2.8, p = 0.07) (data not shown).

To further corroborate these findings, we established a second murine orthotopic PDAC model using Han4.13 cells isolated from Ptf1-Cre; LSL-KRAS-G12D; $p53^{Lox/+}$ mice on and FVB background. In this model, tumors grew to 5–8 mm in maximal diameter by day 14. FOLFIRINOX treatment was similarly associated with a significant decrease in tumor weight (0.21 ± 0.05 g vs. 0.14 ± 0.03 g, p= 0.018), and a significant increase in tumor fibrosis compared to untreated tumors as measured by CPA (13.4 ± 3.7% vs. 17.1 ± 2.8%, p = 0.042) (Supplementary Figure 4A). We evaluated the kinetics of tumor enhancement for Gd-DOTA and CM-101 in FOLFIRINOX-treated animals by measuring MR signal loss over time. Percent ΔSNR values were measured post probe injection and were normalized to peak enhancement at 5 minutes. At 25 minutes post-injection, Gd-DOTA was cleared from the tumor whereas CM-101 was largely retained ($AUC_{5–25}$ 67.5 ± 17.8% vs. 100.1 ± 11.6%, p = 0.0037), indicative of selective binding and retention of CM-101 in regions of fibrotic tumor tissue (Supplemetary Figure 4B). In surrounding pancreas, there was no significant difference in MRI $AUC_{5–25}$ between CM-101 and Gd-DOTA (Supplementary Figure 4C). The corresponding signal retention maps display the relative MR signal intensity at 25 minutes post injection (normalized to peak intensity at 5 minutes) on a color-transformed, pixel-wise basis (Supplementary Figure 4D&E). Finally, we observed that the $AUC_{5–25}$ for CM-101 was significantly greater with FOLFIRINOX compared to the untreated mice (76.2 ± 16.0% vs. 100.1± 11.6%, p = 0.018) (Supplementary Figure 4F). There was no difference in MRI $AUC_{5–25}$ of CM-101 with or without FOLFIRNOX in the adjacent pancreas (Supplementary Figure 4G).

Taken together, these findings indicate that CM-101 selectively binds fibrotic tumor tissue after FOLFIRINOX treatment, resulting in significantly increased MR signal intensity and increased MR $AUC_{5–25}$, which can be correlated to histologic and biochemical measurements of increased collagen deposition in response to cytotoxic chemotherapy. In contrast, there was no change in Gd-DOTA MR signal intensity or $AUC_{5–25}$ after FOLFIRINOX treatment.

Discussion

In this study, we showed that collagen molecular imaging may be a useful technology for assessing treatment response in PDAC, and by extension of our human fibrosis data, might also have prognostic value. In a murine orthotopic PDAC model, we showed that collagen molecular MRI with CM-101 provides three advantages over the standard MR contrast agent, Gd-DOTA. First, CM-101 provides selective MR enhancement of PDAC fibrosis

relative to the surrounding pancreas and retroperitoneum, providing superior resolution of the tumor border on imaging. Second, measurement of both CM-101 absolute MR signal enhancement and $AUC_{5–25}$ allow for objective quantification of collagen content in enhancing stromal tumor compartments, which correlates with probe uptake and histologic collagen quantitation measured by CPA. Third, CM-101-based collagen MRI is sufficiently sensitive to distinguish changes in fibrosis in response to chemotherapy in PDAC, providing a novel non-invasive method for objective determination of treatment response. Importantly, CM-101-based MRI is able to provide this additional information without sacrificing the visual-spatial resolution afforded with conventional MRI.

Taken together, these findings indicate that collagen molecular MRI might have two clinical advantages compared to standard imaging techniques. First, due to the inherent fibrotic nature of PDAC, regardless of treatment, there is specific CM-101 probe uptake into tumor tissue relative to surrounding structures. In human patients, this increased enhancement might allow for more accurate determination of tumor borders as well as regions of local invasion, which is particularly useful for evaluating patients with potentially resectable disease. Second, the ability to measure changes in fibrosis as a surrogate measure of treatment response has implications for all disease stages. For patients with borderline resectable or locally advanced PDAC, evidence of a robust fibrotic response after neoadjuvant CRT may provide strong supporting evidence to go forward with surgical exploration, or vice versa. Similarly, there is an increasing array of therapies available to treat patients with advanced PDAC. However, other than radiographic evidence of tumor shrinkage, growth, or new metastases, there is a paucity of information to guide changes in management. Thus, post-treatment changes in fibrosis might provide an additional layer of data to inform further drug treatments.

In addition to collagen molecular MRI, multiple other non-invasive imaging modalities, including standard of care contrast-enhanced CT[33], CT texture analysis (CTTA)[34], dynamic contrast-enhanced CT (DCE-CT)[35], MRI-based diffusion weight imaging (DWI)[36], and positron emission tomography (PET)[37–39], have been evaluated for their capacity to measure treatment response in PDAC. Compared to these modalities, the potential advantages of collagen molecular MRI include: absence of radioactivity, high resolution imaging, and minimal need for underdeveloped radiographic analytic techniques. Collagen molecular MRI could also be coupled with other MR techniques, such as DWI, to provide multimodal data acquisition from a single imaging session. With respect to clinical translation, CM-101 has been evaluated in other animal models of hepatic and cardiac fibrosis and is currently undergoing additional safety and imaging efficacy studies to support an investigational new drug (IND) filing and subsequent clinical trial evaluation.

In addition to evaluating the efficacy of collagen molecular MRI for imaging PDAC, we also evaluated the prognostic significance of tumor fibrosis after neoadjuvant CRT in a cohort of 93 human patients. We pursued this analysis under the premise that increased post-treatment fibrosis might be a surrogate measure of treatment response, thus providing information about the biology of the tumor and subsequent prognosis. Secondly, current pathologic scoring systems for treatment response, which focus primarily on the amount of residual adenocarcinoma, have been shown to lack precision and reproducibility.[15] Although a

pathologic complete response has been correlated with better outcomes, this outcome is uncommon (~6%), as are near-complete responses (~14%).[13,40] Consequently, there is a need for better prediction in patients with near-complete or limited responses, particularly in patients with large tumors, as the T staging component of TNM provides no prognostic value in the neoadjuvant setting for tumors > 2.0 cm.[13] Finally, potential correlation between fibrosis and survival provides a rational basis for testing collagen molecular MRI as a prognostic tool. In this study, we found that the degree of tumor fibrotic response to neoadjuvant CRT indeed predicted survival, which was independent of other clinicopathologic factors on multivariable analysis. These findings indicate that automated, objective fibrosis scoring using digital analysis of Sirius Red-stained tumor sections may provide prognostic information that has previously been underappreciated, and they also provide strong evidence to support further investigation of collagen molecular MRI as a prognostic tool.

Research teams have also evaluated the prognostic significant of PDAC fibrosis in the pre-treatment setting. Wang et al. measured tumor stromal density in 145 PDAC patients treated with surgical resection followed by adjuvant gemcitabine-based chemotherapy.[41] Tumors were stained for collagen and presence of activated pancreatic stellate cells with Masson's trichrome and αSMA immunohistochemical stain, respectively. Highly-dense stroma, as determined by a pathologic scoring system, was associated with longer overall and progression-free survival, indicating that increased basal tumor fibrosis might have a protective effect. Similarly, Torphy et al. evaluated tumor stroma density using a computer automated algorithm in 123 PDAC patients, and observed that a stroma density of greater than 60% surface area (median value) was associated with significantly improved recurrence-free survival (median 21.1 vs. 10.0 months, $p = 0.008$) and overall survival (median 21.3 vs. 11.7 months, $p = 0.003$) compared to patients with stoma density less than 60%.[42] Finally, Erkan et al. developed a tumor scoring system called the activated stroma index (ASI) that is based on patterns of collagen deposition relative to pancreatic stellate cell activity.[43] They observed that patients with low stellate cell activity, measured by αSMA staining, and high type I collagen deposition had better median overall survival (25.7 mo vs. 16.1 mo, $p = 0.007$). Taken together, these findings indicate that higher levels of basal tumor fibrosis are likely associated with improved survival. Future studies are needed to determine whether baseline tumor fibrosis has any association with response to neoadjuvant therapy and subsequent post-treatment fibrosis.

While our results suggest that collagen molecular MRI is a promising strategy for assessing therapeutic response, there are several important limitations to this study. First, regarding our analysis of human tumor data, the patient cohort was limited to 93 tumor samples and is likely underpowered for certain prognostic associations with small effect size. Second, all patients in this study had localized disease and therefore, our findings are not translatable to the metastatic context. It has been previously reported that differences in tumor fibrosis may exist between primary and metastatic PDAC lesions.[42] Third, all patients were treated with neoadjuvant FOLFIRINOX and radiation therapy, and therefore, this study does not account for the prognostic significance of baseline tumor fibrosis. Future studies are needed to evaluate CPA in the untreated and chemotherapy only contexts. Fourth, regarding PDAC fibrosis imaging with CM-101, these experiments were performed using a murine orthotopic

model of PDAC in a single arm fashion with limited controls due to the complexity of animal MR imaging. Therefore, although we have demonstrated a measurable fibrotic response to therapy, future studies in other animal models of PDAC will be necessary for validation of the CM-101 probe as a useful means of fibrosis imaging. Fifth, in our animal model we only treated with FOLFIRINOX chemotherapy prior to imaging due to complexity of the animal model. Combination FOLFIRINOX with radiotherapy is associated with a more robust fibrotic response that will need to be assessed in future investigations. Chemotherapy alone is still used in some patients, and both chemotherapy and radiotherapy are thought to independently induce fibrosis. Therefore, future human studies are needed to determine whether the association between post-treatment fibrosis and survival is applicable to monotherapy as well. Lastly, more work is needed to correlate the observed fibrotic changes on MRI with pathologic markers of treatment response and prognosis. In this regard, a reproducible scoring system for measuring MR image fibrosis is needed for any potential future clinical translation.

In conclusion, collagen molecular MRI with CM-101 provided superior pancreatic tumor enhancement compared to the non-specific contrast agent, Gd-DOTA. CM-101 is able to detect changes in tissue fibrosis after FOLFIRINOX chemotherapy, providing a novel non-invasive biomarker for treatment response. Based on these preliminary findings in mice, collagen molecular MRI may have additional clinical applications in PDAC including diagnosis and prognostication.

Supplementary Material

Refer to Web version on PubMed Central for supplementary material.

Funding Sources:

This research was supported by the following funding sources: NIH T32CA071345, NIH R01DK104956, R01DK121789, and the Americas Hepato-pancreato-biliary Association (AHPBA) Annual Resident Research Fellowship Grant.

Abbreviations

ASA PS	American Society of Anesthesiologists Physical Status
$AUC_{5–25}$	area under the curve 5–25 minutes post contrast injection
BMI	body mass index
CAP	College of American Pathologists
CPA	collagen proportional area
CT	computed tomography
CTTA	CT texture analysis
Gd-DOTA	gadolinium-1,4,7,10-tetraazacyclododecane-1,4,7,10-tetraacetate

DFS	disease-free survival
DWI	diffusion weighted imaging
EBL	estimated blood loss
ECOG	Eastern Cooperative Oncology Group
Eu	Europium
FDG	18-flourodeoxyglucose
FOLFIRINOX	fluorouracil (5-FU), leucovorin, irinotecan, and oxaliplatin
Gd	Gadolinium
HPA	hydroxyproline analysis
ICP-MS	inductively coupled plasma mass spectrometry
IORT	intraoperative radiation therapy
LVI	lymphovascular invasion
MRI	magnetic resonance imaging
OS	overall survival
PDAC	pancreatic ductal adenocarcinoma
PET	positron emission tomography
PNI	perineural invasion
RECIST	response evaluation cirteria in solid tumors
SD	standard deviation
SEM	standard error of the mean
SMA	smooth muscle actin
SNR	signal-to-noise ratio

References

1. Siegel RL, Miller KD, Jemal A. Cancer Statistics, 2017. CA Cancer J Clin 2017;67:7–30. [PubMed: 28055103]
2. Stark AP, Sacks GD, Rochefort MM, Donahue TR, Reber HA, Tomlinson JS, Dawson DW, Eibl G, Hines OJ. Long-term survival in patients with pancreatic ductal adenocarcinoma. Surgery 2016;159:1520–7. [PubMed: 26847803]
3. Seufferlein T, Bachet JB, Van Cutsem E, Rougier P, Group EGW. Pancreatic adenocarcinoma: ESMO-ESDO Clinical Practice Guidelines for diagnosis, treatment and follow-up. Ann Oncol 2012;23 Suppl 7:vii33–40. [PubMed: 22997452]

4. Lim KH, Chung E, Khan A, Cao D, Linehan D, Ben-Josef E, Wang-Gillam A. Neoadjuvant therapy of pancreatic cancer: the emerging paradigm? The oncologist 2012;17:192–200. [PubMed: 22250057]

5. Heinemann V, Haas M, Boeck S. Neoadjuvant treatment of borderline resectable and non-resectable pancreatic cancer. Annals of oncology : official journal of the European Society for Medical Oncology / ESMO 2013;24:2484–92.

6. Ghaneh P, Kleeff J, Halloran CM, Raraty M, Jackson R, Melling J, Jones O, Palmer DH, Cox TF, Smith CJ, O'Reilly DA, Izbicki JR, Scarfe AG, Valle JW, McDonald AC, Carter R, Tebbutt NC, Goldstein D, Padbury R, Shannon J, Dervenis C, Glimelius B, Deakin M, Anthoney A, Lerch MM, Mayerle J, Olah A, Rawcliffe CL, Campbell F, Strobel O, Buchler MW, Neoptolemos JP, European Study Group for Pancreatic C. The Impact of Positive Resection Margins on Survival and Recurrence Following Resection and Adjuvant Chemotherapy for Pancreatic Ductal Adenocarcinoma. Ann Surg 2017.

7. Michelakos T, Pergolini I, Castillo CF, Honselmann KC, Cai L, Deshpande V, Wo JY, Ryan DP, Allen JN, Blaszkowsky LS, Clark JW, Murphy JE, Nipp RD, Parikh A, Qadan M, Warshaw AL, Hong TS, Lillemoe KD, Ferrone CR. Predictors of Resectability and Survival in Patients with Borderline and Locally Advanced Pancreatic Cancer who Underwent Neoadjuvant Treatment with FOLFIRINOX. Ann Surg 2017.

8. Ferrone CR, Marchegiani G, Hong TS, Ryan DP, Deshpande V, McDonnell EI, Sabbatino F, Santos DD, Allen JN, Blaszkowsky LS, Clark JW, Faris JE, Goyal L, Kwak EL, Murphy JE, Ting DT, Wo JY, Zhu AX, Warshaw AL, Lillemoe KD, Fernandez-del Castillo C. Radiological and surgical implications of neoadjuvant treatment with FOLFIRINOX for locally advanced and borderline resectable pancreatic cancer. Ann Surg 2015;261:12–7. [PubMed: 25599322]

9. Artinyan A, Anaya DA, McKenzie S, Ellenhorn JD, Kim J. Neoadjuvant therapy is associated with improved survival in resectable pancreatic adenocarcinoma. Cancer 2011;117:2044–9. [PubMed: 21523715]

10. Ohigashi H, Ishikawa O, Eguchi H, Takahashi H, Gotoh K, Yamada T, Yano M, Nakaizumi A, Uehara H, Tomita Y, Nishiyama K. Feasibility and efficacy of combination therapy with preoperative full-dose gemcitabine, concurrent three-dimensional conformal radiation, surgery, and postoperative liver perfusion chemotherapy for T3-pancreatic cancer. Ann Surg 2009;250:88–95. [PubMed: 19561477]

11. Evans DB, Varadhachary GR, Crane CH, Sun CC, Lee JE, Pisters PW, Vauthey JN, Wang H, Cleary KR, Staerkel GA, Charnsangavej C, Lano EA, Ho L, Lenzi R, Abbruzzese JL, Wolff RA. Preoperative gemcitabine-based chemoradiation for patients with resectable adenocarcinoma of the pancreatic head. J Clin Oncol 2008;26:3496–502. [PubMed: 18640930]

12. Versteijne E, van Eijck CH, Punt CJ, Suker M, Zwinderman AH, Dohmen MA, Groothuis KB, Busch OR, Besselink MG, de Hingh IH, Ten Tije AJ, Patijn GA, Bonsing BA, de Vos-Geelen J, Klaase JM, Festen S, Boerma D, Erdmann JI, Molenaar IQ, van der Harst E, van der Kolk MB, Rasch CR, van Tienhoven G, Dutch Pancreatic Cancer G. Preoperative radiochemotherapy versus immediate surgery for resectable and borderline resectable pancreatic cancer (PREOPANC trial): study protocol for a multicentre randomized controlled trial. Trials 2016;17:127. [PubMed: 26955809]

13. Chatterjee D, Katz MH, Foo WC, Sundar M, Wang H, Varadhachary GR, Wolff RA, Lee JE, Maitra A, Fleming JB, Rashid A, Wang H. Prognostic Significance of New AJCC Tumor Stage in Patients With Pancreatic Ductal Adenocarcinoma Treated With Neoadjuvant Therapy. Am J Surg Pathol 2017;41:1097–104. [PubMed: 28614206]

14. Chatterjee D, Katz MH, Rashid A, Varadhachary GR, Wolff RA, Wang H, Lee JE, Pisters PW, Vauthey JN, Crane C, Gomez HF, Abbruzzese JL, Fleming JB, Wang H. Histologic grading of the extent of residual carcinoma following neoadjuvant chemoradiation in pancreatic ductal adenocarcinoma: a predictor for patient outcome. Cancer 2012;118:3182–90. [PubMed: 22028089]

15. S NK, Serra S, Dhani N, Hafezi-Bakhtiari S, Szentgyorgyi E, Vajpeyi R, Chetty R. Regression grading in neoadjuvant treated pancreatic cancer: an interobserver study. J Clin Pathol 2017;70:237–43. [PubMed: 27681847]

16. Takahashi H, Ohigashi H, Ishikawa O, Eguchi H, Gotoh K, Yamada T, Nakaizumi A, Uehara H, Tomita Y, Nishiyama K, Yano M. Serum CA19–9 alterations during preoperative gemcitabine-based chemoradiation therapy for resectable invasive ductal carcinoma of the pancreas as an indicator for therapeutic selection and survival. Annals of surgery 2010;251:461–9. [PubMed: 20134315]

17. Katz MH, Fleming JB, Bhosale P, Varadhachary G, Lee JE, Wolff R, Wang H, Abbruzzese J, Pisters PW, Vauthey JN, Charnsangavej C, Tamm E, Crane CH, Balachandran A. Response of borderline resectable pancreatic cancer to neoadjuvant therapy is not reflected by radiographic indicators. Cancer 2012;118:5749–56. [PubMed: 22605518]

18. Ferrone CR, Marchegiani G, Hong TS, Ryan DP, Deshpande V, McDonnell EI, Sabbatino F, Santos DD, Allen JN, Blaszkowsky LS, Clark JW, Faris JE, Goyal L, Kwak EL, Murphy JE, Ting DT, Wo JY, Zhu AX, Warshaw AL, Lillemoe KD, Fernandez-del Castillo C. Radiological and surgical implications of neoadjuvant treatment with FOLFIRINOX for locally advanced and borderline resectable pancreatic cancer. Ann Surg 2015;261:12–7. [PubMed: 25599322]

19. Cassinotto C, Cortade J, Belleannee G, Lapuyade B, Terrebonne E, Vendrely V, Laurent C, Sa-Cunha A. An evaluation of the accuracy of CT when determining resectability of pancreatic head adenocarcinoma after neoadjuvant treatment. Eur J Radiol 2013;82:589–93. [PubMed: 23287712]

20. Polasek M, Yang Y, Schuhle DT, Yaseen MA, Kim YR, Sung YS, Guimaraes AR, Caravan P. Molecular MR imaging of fibrosis in a mouse model of pancreatic cancer. Sci Rep 2017;7:8114. [PubMed: 28808290]

21. Farrar CT, Gale EM, Kennan R, Ramsay I, Masia R, Arora G, Looby K, Wei L, Kalpathy-Cramer J, Bunzel MM, Zhang C, Zhu Y, Akiyama TE, Klimas M, Pinto S, Diyabalanage H, Tanabe KK, Humblet V, Fuchs BC, Caravan P. CM-101: Type I Collagen-targeted MR Imaging Probe for Detection of Liver Fibrosis. Radiology 2017:170595.

22. Murphy JE, Wo JY, Ryan DP, Jiang W, Yeap BY, Drapek LC, Blaszkowsky LS, Kwak EL, Allen JN, Clark JW, Faris JE, Zhu AX, Goyal L, Lillemoe KD, DeLaney TF, Fernandez-Del Castillo C, Ferrone CR, Hong TS. Total Neoadjuvant Therapy With FOLFIRINOX Followed by Individualized Chemoradiotherapy for Borderline Resectable Pancreatic Adenocarcinoma: A Phase 2 Clinical Trial. JAMA Oncol 2018;4:963–9. [PubMed: 29800971]

23. Ryan R, Gibbons D, Hyland JM, Treanor D, White A, Mulcahy HE, O'Donoghue DP, Moriarty M, Fennelly D, Sheahan K. Pathological response following long-course neoadjuvant chemoradiotherapy for locally advanced rectal cancer. Histopathology 2005;47:141–6. [PubMed: 16045774]

24. Farrar CT, DePeralta DK, Day H, Rietz TA, Wei L, Lauwers GY, Keil B, Subramaniam A, Sinskey AJ, Tanabe KK, Fuchs BC, Caravan P. 3D molecular MR imaging of liver fibrosis and response to rapamycin therapy in a bile duct ligation rat model. J Hepatol 2015;63:689–96. [PubMed: 26022693]

25. Zhu B, Wei L, Rotile N, Day H, Rietz T, Farrar CT, Lauwers GY, Tanabe KK, Rosen B, Fuchs BC, Caravan P. Combined magnetic resonance elastography and collagen molecular magnetic resonance imaging accurately stage liver fibrosis in a rat model. Hepatology 2017;65:1015–25. [PubMed: 28039886]

26. Fuchs BC, Wang H, Yang Y, Wei L, Polasek M, Schuhle DT, Lauwers GY, Parkar A, Sinskey AJ, Tanabe KK, Caravan P. Molecular MRI of collagen to diagnose and stage liver fibrosis. J Hepatol 2013;59:992–8. [PubMed: 23838178]

27. Polasek M, Fuchs BC, Uppal R, Schuhle DT, Alford JK, Loving GS, Yamada S, Wei L, Lauwers GY, Guimaraes AR, Tanabe KK, Caravan P. Molecular MR imaging of liver fibrosis: a feasibility study using rat and mouse models. J Hepatol 2012;57:549–55. [PubMed: 22634342]

28. Aguirre AJ, Bardeesy N, Sinha M, Lopez L, Tuveson DA, Horner J, Redston MS, DePinho RA. Activated Kras and Ink4a/Arf deficiency cooperate to produce metastatic pancreatic ductal adenocarcinoma. Genes Dev 2003;17:3112–26. [PubMed: 14681207]

29. Bardeesy N, Aguirre AJ, Chu GC, Cheng KH, Lopez LV, Hezel AF, Feng B, Brennan C, Weissleder R, Mahmood U, Hanahan D, Redston MS, Chin L, Depinho RA. Both p16(Ink4a) and the p19(Arf)-p53 pathway constrain progression of pancreatic adenocarcinoma in the mouse. Proc Natl Acad Sci U S A 2006;103:5947–52. [PubMed: 16585505]

30. Erstad DJ, Sojoodi M, Taylor MS, Ghoshal S, Razavi AA, Graham-O'Regan KA, Bardeesy N, Ferrone CR, Lanuti M, Caravan P, Tanabe KK, Fuchs BC. Orthotopic and heterotopic murine models of pancreatic cancer and their different responses to FOLFIRINOX chemotherapy. Dis Model Mech 2018;11.

31. Chen HH, Waghorn PA, Wei L, Tapias LF, Schu Hle DT, Rotile NJ, Jones CM, Looby RJ, Zhao G, Elliott JM, Probst CK, Mino-Kenudson M, Lauwers GY, Tager AM, Tanabe KK, Lanuti M, Fuchs BC, Caravan P. Molecular imaging of oxidized collagen quantifies pulmonary and hepatic fibrogenesis. JCI Insight 2017;2.

32. Caravan P, Yang Y, Zachariah R, Schmitt A, Mino-Kenudson M, Chen HH, Sosnovik DE, Dai G, Fuchs BC, Lanuti M. Molecular magnetic resonance imaging of pulmonary fibrosis in mice. Am J Respir Cell Mol Biol 2013;49:1120–6. [PubMed: 23927643]

33. Amer AM, Zaid M, Chaudhury B, Elganainy D, Lee Y, Wilke CT, Cloyd J, Wang H, Maitra A, Wolff RA, Varadhachary G, Overman MJ, Lee JE, Fleming JB, Tzeng CW, Katz MH, Holliday EB, Krishnan S, Minsky BD, Herman JM, Taniguchi CM, Das P, Crane CH, Le O, Bhosale P, Tamm EP, Koay EJ. Imaging-based biomarkers: Changes in the tumor interface of pancreatic ductal adenocarcinoma on computed tomography scans indicate response to cytotoxic therapy. Cancer 2018;124:1701–9. [PubMed: 29370450]

34. Ganeshan B, Goh V, Mandeville HC, Ng QS, Hoskin PJ, Miles KA. Non-small cell lung cancer: histopathologic correlates for texture parameters at CT. Radiology 2013;266:326–36. [PubMed: 23169792]

35. Eriksen RO, Strauch LS, Sandgaard M, Kristensen TS, Nielsen MB, Lauridsen CA. Dynamic Contrast-Enhanced CT in Patients with Pancreatic Cancer. Diagnostics (Basel) 2016;6.

36. Niwa T, Ueno M, Ohkawa S, Yoshida T, Doiuchi T, Ito K, Inoue T. Advanced pancreatic cancer: the use of the apparent diffusion coefficient to predict response to chemotherapy. Br J Radiol 2009;82:28–34. [PubMed: 19095814]

37. Baliyan V, Kordbacheh H, Parakh A, Kambadakone A. Response assessment in pancreatic ductal adenocarcinoma: role of imaging. Abdom Radiol (NY) 2017.

38. Kittaka H, Takahashi H, Ohigashi H, Gotoh K, Yamada T, Tomita Y, Hasegawa Y, Yano M, Ishikawa O. Role of (18)F-fluorodeoxyglucose positron emission tomography/computed tomography in predicting the pathologic response to preoperative chemoradiation therapy in patients with resectable T3 pancreatic cancer. World J Surg 2013;37:169–78. [PubMed: 22955953]

39. Yoshioka M, Sato T, Furuya T, Shibata S, Andoh H, Asanuma Y, Hatazawa J, Shimosegawa E, Koyama K, Yamamoto Y. Role of positron emission tomography with 2-deoxy-2-[18F]fluoro-D-glucose in evaluating the effects of arterial infusion chemotherapy and radiotherapy on pancreatic cancer. J Gastroenterol 2004;39:50–5. [PubMed: 14767734]

40. He J, Blair AB, Groot VP, Javed AA, Burkhart RA, Gemenetzis G, Hruban RH, Waters KM, Poling J, Zheng L, Laheru D, Herman JM, Makary MA, Weiss MJ, Cameron JL, Wolfgang CL. Is a Pathological Complete Response Following Neoadjuvant Chemoradiation Associated With Prolonged Survival in Patients With Pancreatic Cancer? Ann Surg 2018.

41. Wang LM, Silva MA, D'Costa Z, Bockelmann R, Soonawalla Z, Liu S, O'Neill E, Mukherjee S, McKenna WG, Muschel R, Fokas E. The prognostic role of desmoplastic stroma in pancreatic ductal adenocarcinoma. Oncotarget 2016;7:4183–94. [PubMed: 26716653]

42. Torphy RJ, Wang Z, True-Yasaki A, Volmar KE, Rashid N, Yeh B, Anderson JM, Johansen JS, Hollingsworth MA, Yeh JJ, Collisson EA. Stromal Content Is Correlated With Tissue Site, Contrast Retention, and Survival in Pancreatic Adenocarcinoma. JCO Precis Oncol 2018;2018.

43. Erkan M, Michalski CW, Rieder S, Reiser-Erkan C, Abiatari I, Kolb A, Giese NA, Esposito I, Friess H, Kleeff J. The activated stroma index is a novel and independent prognostic marker in pancreatic ductal adenocarcinoma. Clin Gastroenterol Hepatol 2008;6:1155–61. [PubMed: 18639493]

Statement of Significance:

We show that the fibrotic response to neoadjuvant chemoradiation in PDAC is associated with overall and disease-free survival, and secondly that preclinical murine experiments indicate that collagen molecular MRI can be used to non-invasively measure the fibrotic response to therapy in order to guide management.

Statement of Translational Relevance:

We describe two techniques that have potential for clinical impact. The first technique is collagen targeted MRI of pancreatic ductal adenocarcinoma (PDAC). Standard CT and MRI are unable to distinguish chemoradiation induced fibrotic response from residual cancer, complicating management. We demonstrate that collagen targeted MRI in an orthotopic murine model of PDAC provides superior tumor enhancement and can be used to measure post-treatment fibrotic changes in the tumor bed. Although preliminary, these findings suggest that collagen targeted MRI might have clinical utility to evaluate response to chemoradiation and may help with downstaging. The second technique uses Sirius Red collagen staining to measure fibrosis in chemoradiation-treated tumors. Current pathologic scoring systems focus on quantifying residual adenocarcinoma, and lack reproducibility and prognostic value. In contrast, we show that objective fibrosis quantification of the post-chemoradiation tumor bed is associated with survival and is a more accurate prognostic marker than either pathologic regression grade or RECIST score in a single-center study of 93 human patients.

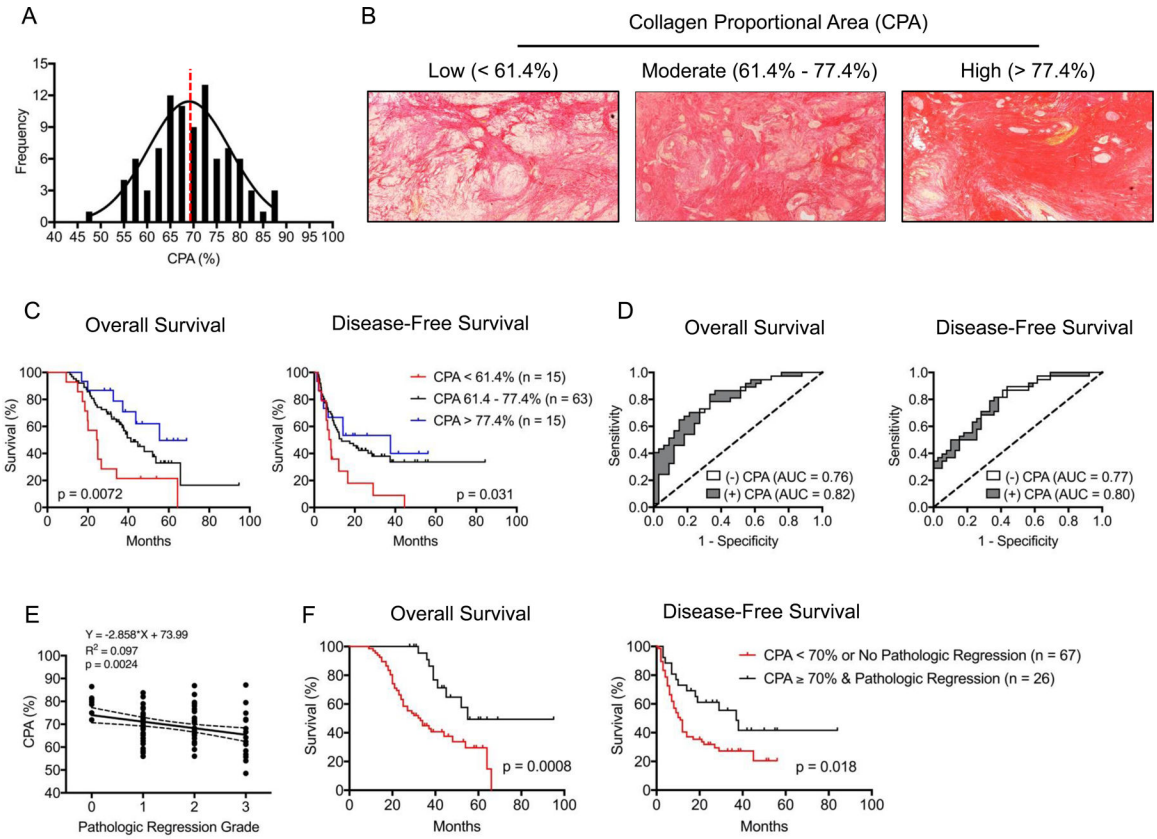

Figure 1:

(A) Frequency distribution plot for tumor fibrosis levels measured by digital quantification of Sirius Red collagen staining. Dashed red line separates patients by CPA < 70% or ≥ 70%. **(B)** Sirius Red collagen staining of tumor samples representing low (CPA < 61.4%), moderate (61.4% −77.4%), and high (CPA > 77.4%) fibrosis groups. Residual cancer cells occupy regions of non-fibrotic tissue. Kaplan-Meier survival curves based on **(C)** CPA stratified into low (CPA < 61.4%, red), moderate (61.4% −77.4%, black), and high (CPA > 77.4%, blue) fibrosis groups. **(D)** Logistic regression model for prediction of median OS and DFS including (gray) and excluding (white) CPA as a variable. **(E)** Correlation between CPA (%) and pathologic regression grading (tumor regression grades: 0 = complete response, no viable tumor cells; 1 = moderate response, single small cells or groups of cells; 2 = minimal response, residual cancer outgrown by fibrosis; 3 = poor response, minimal or no tumor kill, extensive residual cancer. **(F)** Kaplan-Meier survival curves for OS and DFS stratified by CPA < 70 & no pathologic response (regression grade 2 – 3) (red) compared to CPA ≥ 70% & pathologic response (regression grade 0 – 1) (black).

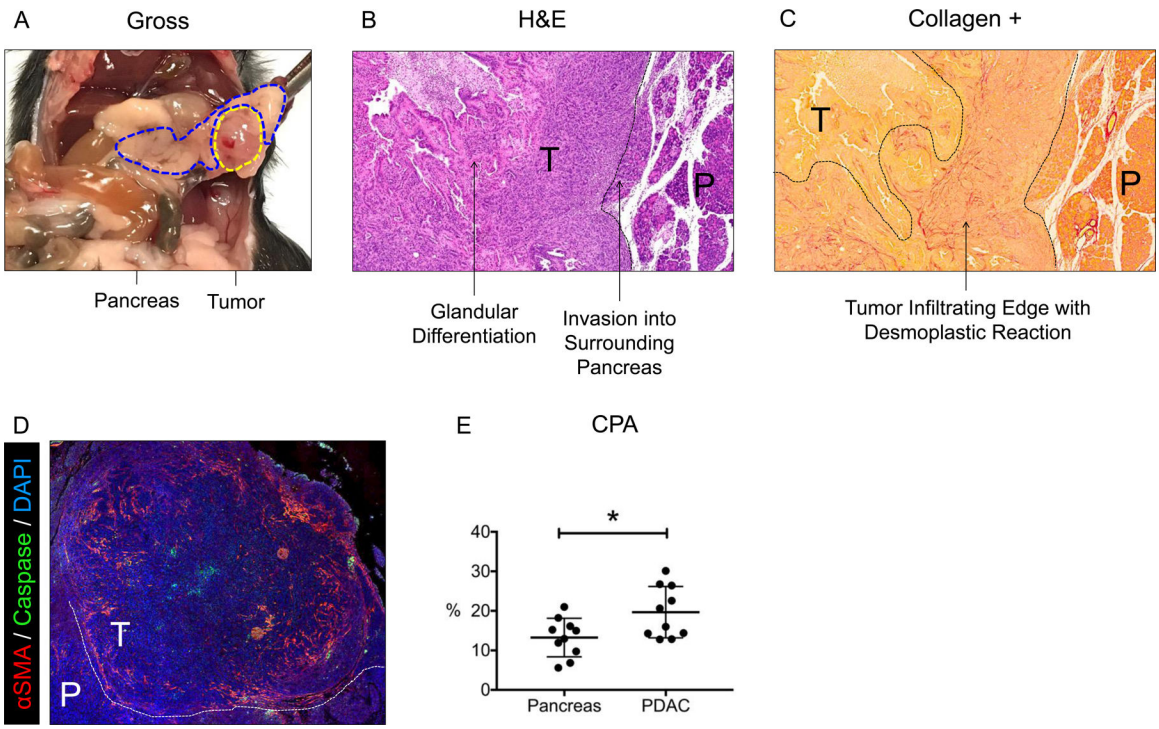

Figure 2:

(A) Gross image of pancreas (blue dotted line) and PDAC tumor (yellow dotted line) 14 days after orthotopic injection. **(B)** Hematoxylin and eosin (H&E) staining of the tumor and surrounding pancreas. Histologic features are labeled with arrows. **(C)** Sirius Red staining of the tumor and surrounding pancreas. Desmoplastic reaction at the tumor's infiltrating edge is indicated by intense red stain (increased collagen density). **(D)** Immunofluorescent staining of αSMA in tumor and surrounding pancreas. **(E)** Collagen proportional area (CPA) of tumor and surrounding pancreatic tissue. T = tumor; P = pancreas. * $p < 0.05$; ** $p < 0.01$.

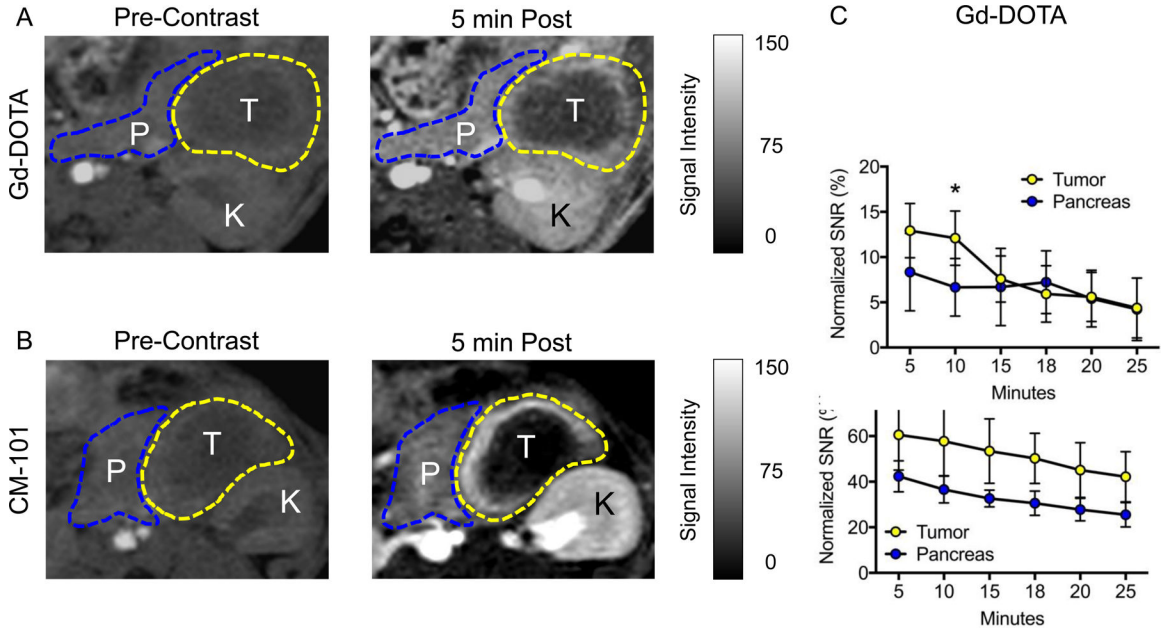

Figure 3:

Representative axial images of orthotopically implanted tumors (yellow dotted line) and surrounding pancreas (blue dotted line) pre and 5 minutes post Gd-DOTA **(A)** and CM-101 **(B)** contrast injections. %ΔSNR in PDAC and surrounding pancreas at all measured time points for **(C)** Gd-DOTA and **(D)** CM-101. T = tumor; P = pancreas; K = kidney. * $p < 0.05$; ** $p < 0.01$.

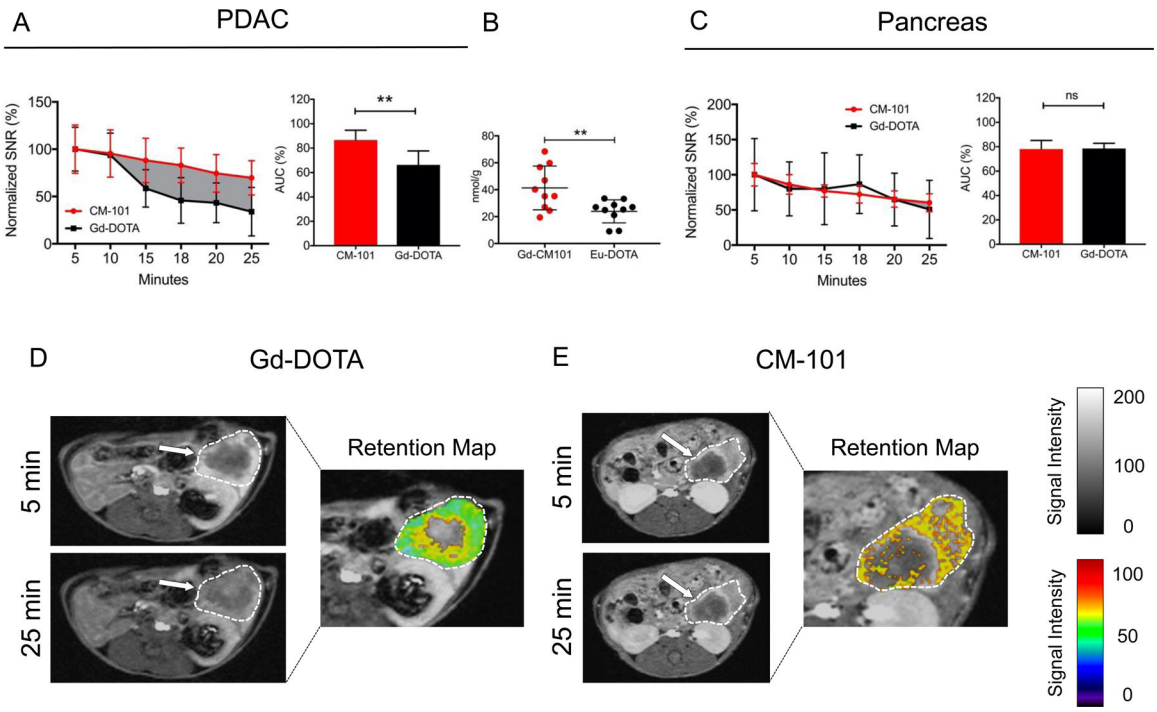

Figure 4:

(A) SNR measurements are normalized to peak intensity at 5 minutes. Plotted lines represent Gd-DOTA (black) and CM-101 (red) signal loss over 25 minutes. Relative to peak signal, the MR signal intensity is significantly greater with CM-101 compared to Gd-DOTA from 15–25 minutes. Difference in $AUC_{5–25}$ is graphically displayed by solid gray background. $AUC_{5–25}$ for the Gd-DOTA and CM-101 are shown in the bar graph. **(B)** ICP-MS quantitation of Eu-DOTA and CM-101 probes in PDAC tissue 25 minutes after tail vein injection. **(C)** Relative MR signal loss in surrounding pancreatic tissue 5–25 minutes post injection with CM-101 and Gd-DOTA. $AUC_{5–25}$ for Gd-DOTA and CM-101 are shown in the bar graph. **(D)** Representative axial images of untreated PDAC 5 and 25 minutes after Gd-DOTA injection. Tumor is outlined in white (grayscale) and white arrows point to fibrotic tumor regions. Retention map displays MR signal intensity normalized to peak signal at 5 minutes in tumor tissue. **(E)** Representative axial images of untreated PDAC 5 and 25 minutes after CM-101 injection with retention map. * $p < 0.05$; ** $p < 0.01$.

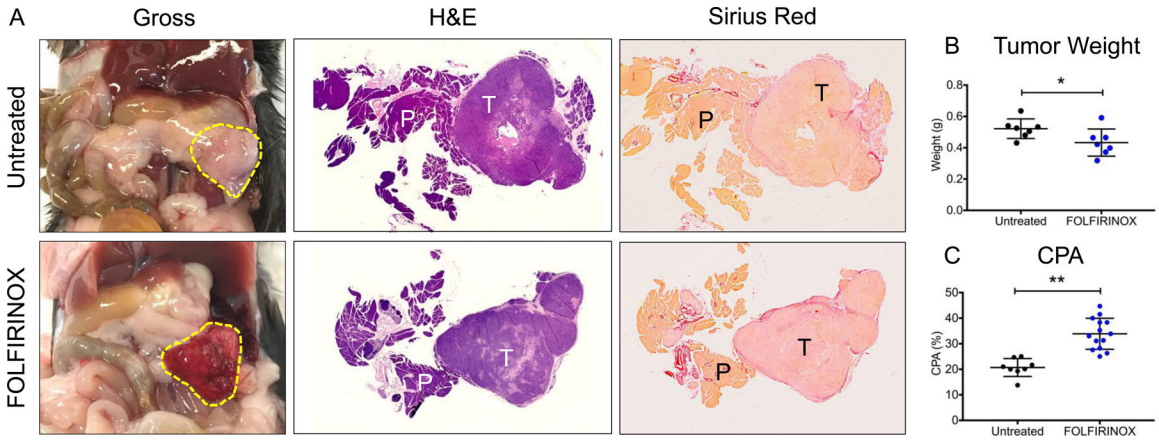

Figure 5:

(A) Gross images of tumor (outline in yellow dotted line), untreated and after 3 doses of FOLIFIRINOX. H&E and Sirius Red collagen staining of tumor and pancreatic tissue are shown. **(B)** Tumor weights in untreated and FOLFIRINOX-treated mice. **(C)** CPA measurements of PDAC tissue for untreated and FOLFIRINOX-treated mice. T = tumor; P = pancreas. * $p < 0.05$; ** $p < 0.01$.

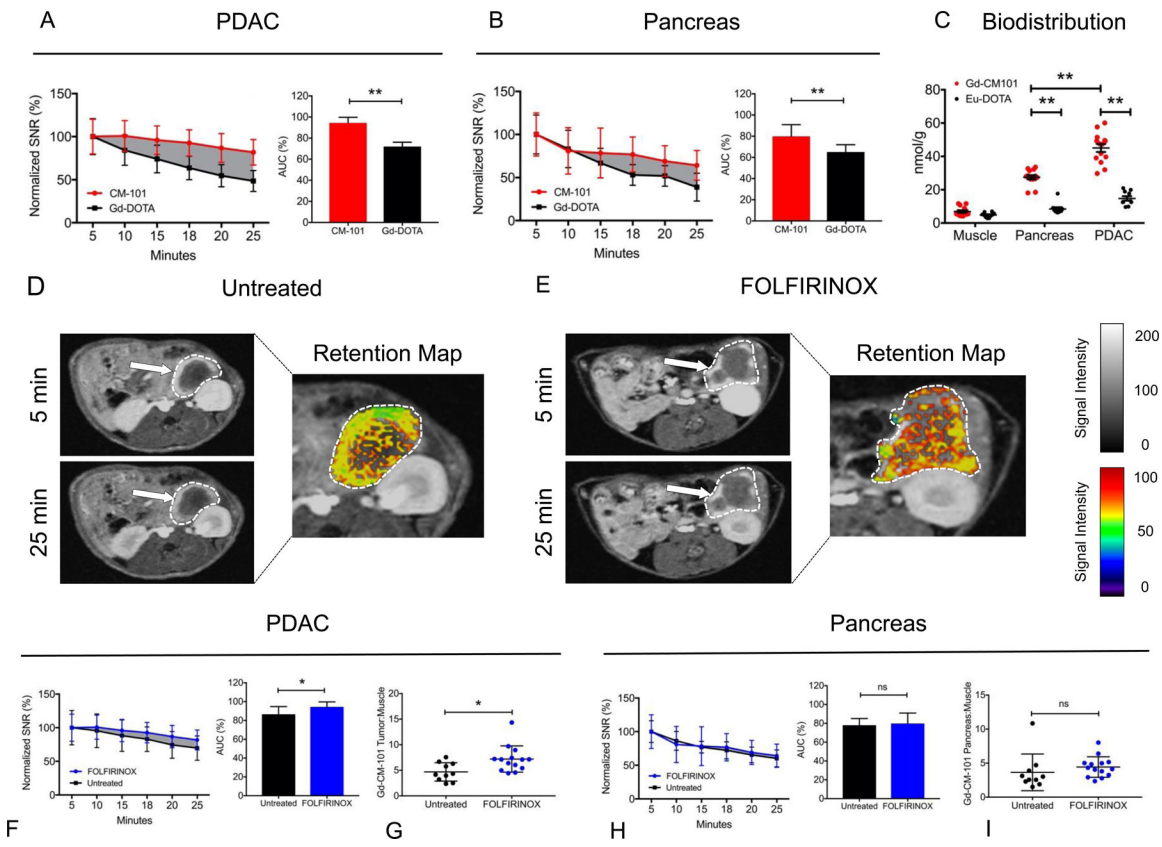

Figure 6:

(A) SNR measurements normalized to peak intensity at 5 minutes post-injection for FOLFIRINOX-treated PDAC. Plotted lines represent Gd-DOTA (black) and CM-101 (red) signal loss over 25 minutes. Relative to peak signal, the MR signal intensity is significantly greater with CM-101 compared to Gd-DOTA from 10–25 minutes. Difference in $AUC_{5–25}$ is graphically displayed by solid gray background. $AUC_{5–25}$ for Gd-DOTA and CM-101 are shown in the bar graph. **(B)** Relative MR signal attenuation in surrounding pancreatic tissue up to 25 minutes post injection with CM-101 and Gd-DOTA after FOLFIRINOX treatment. $AUC_{5–25}$ for Gd-DOTA and CM-101 are shown in the bar graph. **(C)** ICP-MS quantitation of Eu-DOTA and CM-101 probe uptake in muscle, PDAC, and pancreas tissues 25 minutes after tail vein injection in FOLFIRINOX-treated mice. **(D)** Representative axial images of untreated PDAC 5 and 25 minutes after CM-101 injection. Tumor is outlined in white (grayscale) and white arrows point to fibrotic tumor regions. Retention map displays MR signal intensity normalized to peak signal at 5 minutes in tumor tissue. **(E)** Representative axial images of FOLFIRINOX-treated PDAC 5 and 25 minutes after CM-101 injection with retention map. **(F)** CM-101-based MR signal intensity measurements normalized to peak intensity at 5 minutes. Plotted lines represent untreated (black) and FOLFIRINOX-treated (blue) PDAC signal loss over 25 minutes. Difference in $AUC_{5–25}$ is graphically displayed by solid gray background. $AUC_{5–25}$ for CM-101 in untreated and FOLFIRINOX-treated PDAC are shown in the bar graph. ICP-MS quantitation of **(G)** tumor and **(I)** pancreatic tissue CM-101 probe uptake 25 minutes after tail vein injection. **(H)** CM-101 MR signal intensity

measurements for pancreatic tissue in untreated and FOLFIRINOX-treated mice, and associated $AUC_{5–25}$ calculations. * $p < 0.05$; ** $p < 0.01$.

Table 1:

Cohort Data and Univariate Survival Analysis

		Overall Survival (OS)		Disease Free Survival (DFS)	
Variable	**(mean ± SD) or n (%)**	**HR**	**p-value**	**HR**	**p-value**
Demographics					
Age (years)	61.7 ± 8.9	1.01	0.73	1.00	0.98
Gender					
Female	49 (51%)	1.16	0.50	1.03	0.90
Male	47 (49%)				
Race					
Caucasian	88 (94%)	1.50	0.045	1.53	0.041
Black	3 (3%)				
Asian	3 (3%)				
Hispanic	0 (0%)				
BMI	25.8 ± 5.6	0.97	0.32	1.01	0.55
ASA Category		0.87	0.64	0.78	0.35
1	0 (0%)				
2	54 (56%)				
3	42 (44%)				
Charlson Comorbidity Index Score	2.3 ± 2.5	1.07	0.52	1.23	**0.048**
ECOG Score		1.27	0.30	1.18	0.47
0	65 (70%)				
1	27 (29%)				
2	0 (0%)				
3	1 (1%)				
Radiographic and Serum Biomarkers					
Tumor Diameter at Diagnosis (cm)	3.4 ± 1.1	1.47	**0.003**	1.33	**0.013**
RECIST		1.08	0.62	0.97	0.88
Complete Response (CR)	8 (8%)				
Partial Response (PR)	66 (69%)				
Stable Disease (SD)	16 (17%)				
Progressive Disease (PD)	1 (1%)				
Inevaluable	5 (5%)				
Cycles of Chemotherapy	8 ± 2.5	1.02	0.64	1.02	0.58
CA-19–9 at Diagnosis (U/mL; normal < 35)		1.21	0.008	1.28	**0.001**
< 35	30 (34%)				
35 – 100	11 (12%)				
101 – 500	23 (26%)				
501 – 1000	10 (11%)				
> 1000	15 (17%)				

		Overall Survival (OS)		Disease Free Survival (DFS)	
Variable	**(mean ± SD) or n (%)**	**HR**	**p-value**	**HR**	**p-value**
Operative and Pathologic Data					
Pathologic Regression Score		1.53	**0.005**	1.37	**0.032**
Complete Response	7 (7%)				
Moderate Response	42 (44%)				
Minimal Response	29 (30%)				
Poor Response	18 (19%)				
Collagen Proportional Area (CPA, %)	69.4 ± 8.0	0.94	**0.001**	0.95	**0.009**
Pathologic Tumor Diameter (cm)	2.3 ± 1.5	1.45	< **0.0001**	1.22	**0.018**
T stage		1.49	**0.017**	1.26	0.10
0	8 (8%)				
1	10 (10%)				
2	9 (9%)				
3	68 (71%)				
4	1 (1%)				
N stage		1.96	**0.018**	2.18	**0.003**
0	65 (68%)				
1	30 (31%)				
2	1 (1%)				
LVI	21 (22%)	1.56	0.17	1.27	0.45
PNI	59 (63%)	2.28	**0.013**	1.31	0.33
Margin Status		1.35	0.46	1.47	0.31
R0	86 (90%)				
R1	10 (10%)				
EBL (mL)	728 ± 474	1.00	0.91	0.99	0.89
Operative Time	389 ± 121	1.20	0.005	1.11	0.092
Vascular Reconstruction	24 (25%)	0.89	0.72	1.12	0.69
IORT	31 (32%)	0.87	0.65	0.81	0.46
Postoperative Clinical Data					
Adjuvant Chemotherapy	38 (40%)	1.88	**0.027**	3.76	< **0.0001**
Adjuvant Radiotherapy	17 (18%)	1.54	0.21	1.97	**0.033**

ASA PS, American Society of Anesthesiologists Physical Status; BMI, body mass index; College of American Pathologists (CAP) Regression Grades: 0 = complete response, no viable tumor cells; 1 = moderate response, single small cells or groups of cells; 2 = minimal response, residual cancer outgrown by fibrosis; 3 = poor response, minimal or no tumor kill, extensive residual cancer; EBL, estimated blood loss; ECOG, Eastern Cooperative Oncology Group; IORT, intraoperative radiation therapy; LVI, lymphovascular invasion; PNI, perineural invasion; RECIST, response evaluation cirteria in solid tumors; SD, standard deviation.

Table 2:

Multivariable Analysis of Survival Outcome Measures

	Overall Survival		Disease Free Survival	
Variable	**HR**	**p-value**	**HR**	**p-value**
CPA	0.96	**0.028**	0.96	**0.047**
Radiographic Tumor Diameter at Diagnosis	1.38	**0.045**	1.35	**0.023**
CA-19–9	1.16	0.088	0.98	0.10
Pathologic Regression (complete or partial)	0.75	0.49	1.09	0.47
Pathologic Tumor Diameter	1.20	0.16	1.56	0.21
N stage 1–2	1.12	0.80	1.29	0.002
T Stage 3–4	1.14	0.76		
Perineural Invasion	1.14	0.71		

CPA, collagen proportional area.